

# Evaluation of CT-DEA performance on Ca/P ratio assessment in bone apatite using EDX

A. Hadjipanteli,<sup>a\*</sup> N. Kourkoumelis<sup>b</sup> and R. Speller<sup>a</sup>

The aim of this study is to evaluate the performance of a new computed tomography-dual energy analysis (CT-DEA) technique developed for the non-invasive assessment of the 3D spatial distribution of calcium/phosphorus (Ca/P) ratio in bone. For this, the Ca/P ratio in 58 regions from four healthy and four inflammation-mediated osteoporotic (IMO) rabbit bone collagen-free samples were assessed using energy dispersive X-ray spectroscopy (EDX) and CT-DEA. Image registration, performed using NifTK software (Centre for Medical Imaging Computing, University College London), allowed the comparison with the results from the two imaging systems.

A value of  $R^2 = 0.69$  in the fit of CT-DEA Ca/P ratio versus EDX Ca/P ratio and a mean absolute/percentage difference of  $0.11 \pm 0.08/8 \pm 6\%$  in the CT-DEA Ca/P ratio from the EDX results suggest sufficient confidence in the current experimental capabilities of the developed technique. The main difficulties in the comparison of the results using the two techniques and possible sources of error are discussed.

Even though there are still possible improvements that can be made in the developed technique, through this study, it has been shown that CT-DEA can provide valuable 3D, non-invasive information on the comparison between healthy and osteoporotic bone. © 2014 The Authors. *X-Ray Spectrometry* published by John Wiley & Sons, Ltd.

## Introduction

Areal bone mineral density, using dual energy X-ray absorptiometry (DEXA), is the conventional osteoporosis indicator. However, it has some limitations when used to classify bone<sup>[1–3]</sup>, and sometimes physicians face the dilemma of deciding which patients should receive treatments.

The calcium/phosphorus ratio (Ca/P) could be a new osteoporosis indicator. Low and non-homogeneously distributed Ca/P ratio was shown to be correlated to osteoporotic bone<sup>[4,5]</sup> and thus possibly affect bone quality. A computed tomography (CT) post-reconstruction dual energy analysis (CT-DEA) technique was recently developed<sup>[6]</sup> for the non-invasive assessment of the 3D spatial distribution of the Ca/P ratio in bone apatite. This could potentially help in better understanding bone pathogenesis and in providing an enhanced and earlier diagnostic method. CT-DEA was optimised for a micro-computed tomography system (micro-CT), which uses a polychromatic X-ray beam, and was validated using bone phantoms.

In the current study, we evaluate the performance of CT-DEA when used on real bone apatite. Ca/P ratio measurements made on healthy and osteoporotic bone apatite using the technique were compared with measurements made using energy dispersive X-ray spectroscopy (EDX), regularly used for Ca/P ratio measurements on bone surfaces<sup>[7–15]</sup>.

## Method

### Phantoms

For the validation of the EDX measurements, three bone phantoms were used. The bone phantoms were formed using calcium phosphate powders (Sigma-Aldrich Ltd) of three different chemical compositions ( $\text{Ca}(\text{H}_2\text{PO}_4)_2 \cdot \text{H}_2\text{O}$ ,  $\text{CaHPO}_4$ ,  $\text{Ca}_3(\text{PO}_4)_2$ ) and thus Ca/P ratio (Ca/P ratios of 0.5, 1.0 and 1.5, respectively). These were compressed into small cylindrical pellets (diameter 8 mm and

height 2–4 mm) of different densities using a Specac hydraulic presser. The certainty with which the composition was known for the three phantoms was 85%, 98%, and 96%, respectively. As provided by the supplier possible impurities include traces of Cl-anions and traces of metallic cations. For the monohydrate salt, a possible additional impurity is phosphoric acid as indicated in PubChem database<sup>[16]</sup>.

### Samples

Eight cortical bone samples were obtained from two female New Zealand white rabbits to investigate the performance of CT-DEA in Ca/P ratio assessment. All animal experiments were performed at Ioannina University, and all study protocols were approved by the Ioannina University Institutional Animal Care and Use Committee.

Four of the samples were inflammation-mediated osteoporotic (IMO). The inflammation was introduced to one of the animals, at 8 months of age, by injections of talcum (Sigma-Aldrich Ltd) on the back of the rabbit at sites distant from the skeleton, to stimulate an acute phase response<sup>[12,17]</sup>.

The animals were euthanised under light ether anesthesia after 21 days and cortical sections were dissected. EDX measurements can be inaccurate when organic phase is present in samples and

\* Correspondence to: A. Hadjipanteli, Department of Medical Physics and Bioengineering, University College London, Gower Street, London, WC1E 6BT, UK. E-mail: andria.hadjipanteli.09@ucl.ac.uk

a Department of Medical Physics and Bioengineering, University College London, Gower Street, London, WC1E 6BT, UK

b Department of Medical Physics, Medical School, University of Ioannina, Ioannina, 45110, Greece

This is an open access article under the terms of the Creative Commons Attribution License, which permits use, distribution and reproduction in any medium, provided the original work is properly cited.

sometimes carbon coating is suggested. Carbon coating was not used in this study as it has been shown that it is impossible to eliminate the contribution of the carbon coating to the EDX signal when used in samples like bone.<sup>[18]</sup> Instead, all samples were heated at 350°C for 48 h to remove collagen<sup>[19,20]</sup> for the formation of bone apatite samples<sup>[6]</sup>. After heating, the shape of the bone samples was preserved. Heat treatment at below 500°C has no detectable effect on the size, crystallinity, or lattice spacing of the crystals of bone apatite while at the same time it effectively removes most of the organic part<sup>[20]</sup>. All samples were carefully polished using a polishing paper of grit size  $58.5 \pm 2.0 \mu\text{m}$ , to make the surface flat and parallel and thus minimize the topographic effects. A diamond wheel saw could have been used instead for more flat surfaces; however, due to the high fragility of the collagen-free samples, it was avoided.

**CT-DEA**

All bone samples were imaged using a bench-top cone-beam micro-CT system (Nikon Metrology, X-Tek, UK); serial number: J00001. The optimum imaging conditions used for the low and high energies are summarised in Table 1. Scanning parameters were: magnification = 10 360 projections. For each projection, 128 frames were acquired and averaged.

CT reconstruction was performed using the in-built X-Tek software at a slice thickness of  $16 \mu\text{m}$  (Nikon Metrology, X-Tek, UK). Any centre of rotation artefacts were corrected using CT Pro software (Nikon Metrology, X-Tek, UK). Following reconstruction, all sample images were binned into  $6 \times 6 \times 6$  voxels to increase the signal to noise ratio of the images, thus providing a resolution of  $96 \mu\text{m}$  in all dimensions.

The images of all bone samples were processed using the CT-DEA method described in our previous work<sup>[6]</sup>. Briefly, the technique decomposed bone apatite to Ca,  $\text{PO}_4$ , and OH and was based on pre-defined relationships between the ratio of low and high energy CT values for one voxel,  $F(Z_{\text{eff}})$ , to effective atomic number,  $Z_{\text{eff}}$  and  $Z_{\text{eff}}$  to low energy mass attenuation coefficient,  $m_L$ . The latter was decomposed to  $f_{\text{Ca}}, f_P$ , where  $f_i$  represents the fraction by weight of a component  $i$ .

A two-dimensional Ca/P ratio colour map was produced for each sample surface, to allow visual differentiation of areas of low and high Ca/P ratio. Figure 1 shows the original low-energy images [(a) and (c)] and the corresponding Ca/P ratio maps [(b) and (d)] for healthy and IMO rabbit bone samples. Comparing the Ca/P ratio maps, an increased area of low Ca/P ratio in the IMO slice can clearly be noticed. Such differences are not immediately obvious in the original low-energy CT images.

The Ca/P ratio maps were used to identify a total of 58 regions of interest (ROIs), 26 ROIs from the healthy bone samples, and 32 ROIs from the IMO bone samples, covering a wide range of Ca/P ratio, to be validated using EDX. The surface area of these regions was in the range of 0.15–0.23 mm<sup>2</sup>.

**EDX**

Backscatter scanning electron microscopy (SEM) images of the surface of interest of each bone phantom and sample were acquired using an SEM system (Hitachi model S-3400N, Japan); serial number: 340621-04. The imaging conditions for all phantoms and samples were 20 kV, emission current 128  $\mu\text{A}$ , and magnification  $\times 27$ .

The three bone phantoms of different known Ca/P ratio were used for the validation of EDX measurements.

**Table 1.** Conditions used for all imaging performed with the benchtop micro-CT system.

Imaging Condition	Low E Image	High E Image
Voltage (kVp)	50	100
Current ( $\mu\text{A}$ )	150	100
Filter material	Al	Sn
Filter thickness (mm)	5	0.5
Mean energy (keV)	36	71

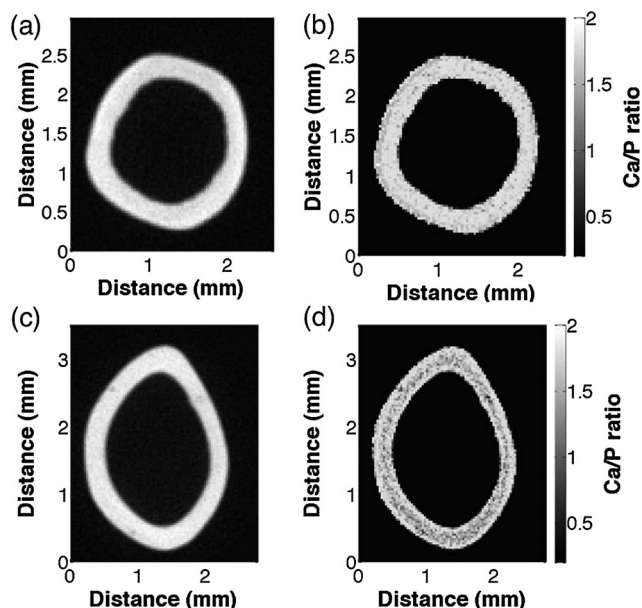


**Figure 1.** Slices extracted from the original low-energy CT images (a) and (c) and their corresponding Ca/P ratio 2D maps (b) and (d) for rabbit bone samples. The samples are healthy (a) and (b) and inflammation-mediated osteoporotic (c) and (d). Each voxel is  $96 \mu\text{m}^3$ .

The approximate ROI of each bone surface, as selected on the CT-DEA Ca/P ratio colour map, were identified on its corresponding SEM backscatter image. The depth within the sample to which the EDX Ca/P ratio results correspond to was estimated to be  $4 \mu\text{m}$ . The spectrum of each ROI was produced, together with a table detailing the sample composition, including  $f_{\text{Ca}}, f_P$ . From this, the Ca/P ratio was then calculated.

**Image registration and analysis**

The Ca/P ratio map and the SEM image of the same sample surface produced from the two imaging systems were of different magnification, pixel size, and sometimes orientation. Image registration was performed to map the CT-DEA Ca/P ratio map to the SEM image. NifTK, a translational imaging platform, developed at the Centre for Medical Image Computing of University College London, was used. The necessary scaling, rotation, and translation amendments were made to the CT-DEA Ca/P ratio map image for its geometry to be mapped sufficiently well on top of the SEM image (Figure 2).

Image registration reproduced the CT-DEA Ca/P ratio map with the grey values of the original CT-DEA Ca/P ratio map and the

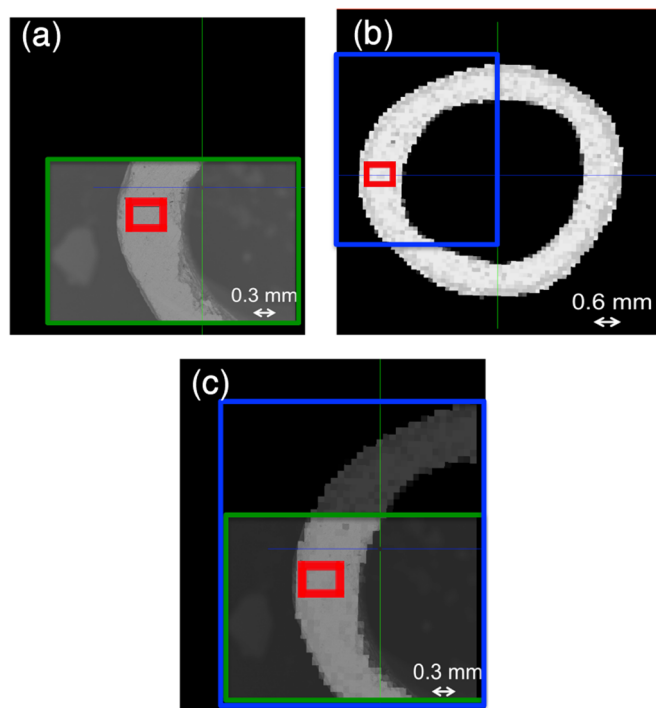


**Figure 2.** (a) Backscatter scanning electron microscopy image, (b) CT-dual energy analysis Ca/P ratio colour map of the surface of an inflammation-mediated osteoporotic bone sample. The mapping of the two images in NifTK is shown in (c).

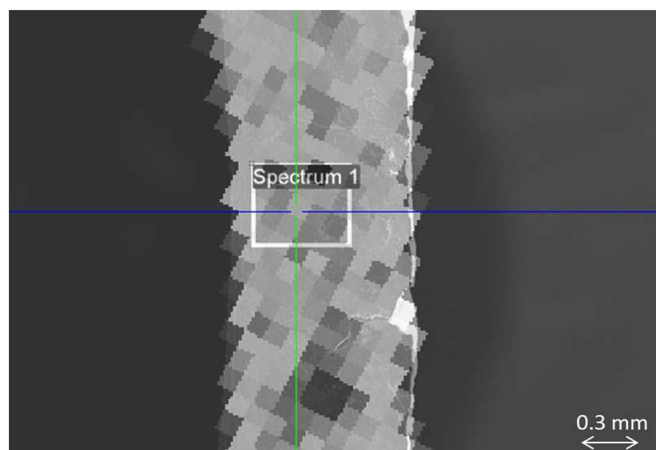


**Figure 3.** A case where there was a misalignment of the pixels of CT image to the pixels of the scanning electron microscopy image, due to the different orientation of the sample to the detector in the two systems.

SEM pixel size and coordinates. The coordinates of each ROI were determined on the registered Ca/P ratio map, and the corresponding coordinates were found on the original Ca/P ratio map. The mean Ca/P ratio by CT-DEA of the ROI was calculated.

In some cases, the coordinates of the CT-DEA Ca/P ratio map registered image were only an approximation to the CT-DEA Ca/P ratio map original image (Figure 3). This was due to the different alignment of the pixels with respect to the sample, which resulted from the different orientation of the sample to the

detector in the two imaging systems. In these cases, all pixels that were within or intersected with the ROIs were used to evaluate the Ca/P ratio mean.

The mean Ca/P ratio of the ROIs was compared with the corresponding SEM Ca/P ratio, using linear regression analysis. Furthermore, a two-sample Student's *t*-test was used to investigate the statistical significance in the difference of the Ca/P ratios of the healthy and IMO areas, using the two different techniques.

## Results and Discussion

### Areal Ca/P ratio assessment using EDX

#### Phantoms

Three bone phantoms were used for the validation of the EDX Ca/P ratio assessment. A typical example of an SEM backscatter bone phantom ( $\text{Ca}(\text{H}_2\text{PO}_4)_2 \cdot \text{H}_2\text{O}$ ) image is shown in Figure 4(a), with a selection of the ROI. Its corresponding spectrum is shown in Figure 4(b). The presence of calcium, phosphorus, and oxygen can be observed as expected. The relative height of the Ca and P peaks is proportional to the Ca/P ratio, provided the matrix effects (atomic number, x-ray absorption and x-ray fluorescence) are taken into account.

The absolute error in the assessment of  $f_{\text{Ca}}$  and  $f_{\text{P}}$  in phantoms by EDX is shown in Figure 5. The mean absolute/percentage difference between the expected and measured  $f_i$  of the three phantoms was  $0.02 \pm 0.02/10 \pm 7\%$ . A possible source of the error is the little effect the ZAF correction procedure (where Z is the effective atomic number, A is the X-ray absorption, and F is fluorescence) has on biological samples especially because of low Z ( $< 20$ ). Good experimental values for the ZAF correction technique are not available for all elements and X-ray lines (particularly for light elements). Therefore, they cannot reliably compensate, especially for A (absorption), mostly because ZAF

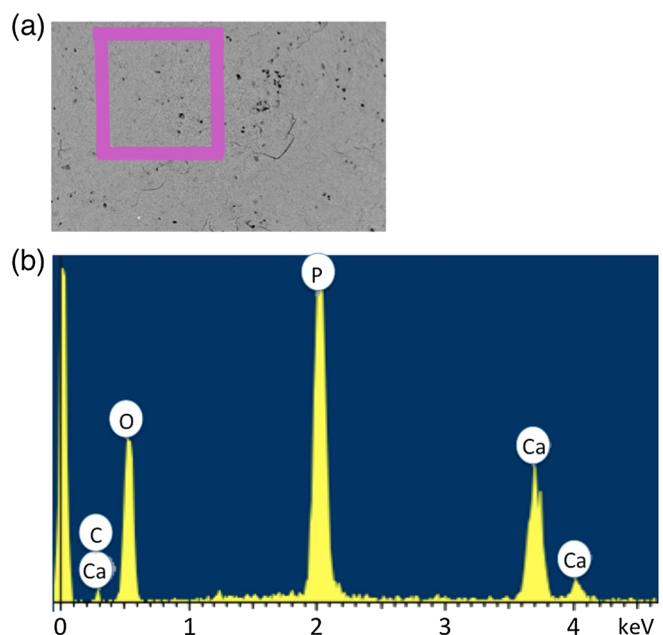


**Figure 4.** (a) Scanning electron microscopy backscatter image, with a selection of the region of interest, and (b) its corresponding energy dispersive X-ray spectroscopy spectrum, acquired using a bone phantom of Ca/P ratio = 0.5.

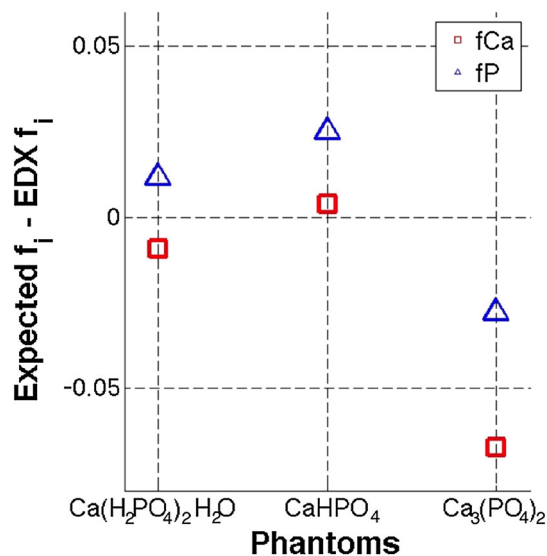


**Figure 5.** Energy dispersive X-ray spectroscopy measurements. Deviation from the expected  $f_{\text{Ca}}$  (blue triangles) and  $f_{\text{P}}$  (pink squares) for phantoms of different Ca/P ratio.

was firstly introduced for metallic standards, which have different mean absorption coefficients from bone. It has been suggested that EDX gives 5–7% error in low Z element results because of the lack or incorrect correction of ZAF<sup>[8,21]</sup>. This partly explains the error in  $f_i$  (10%). The uncertainty with which the composition was known for the three phantoms (4–15%) might partly explain the error, too.

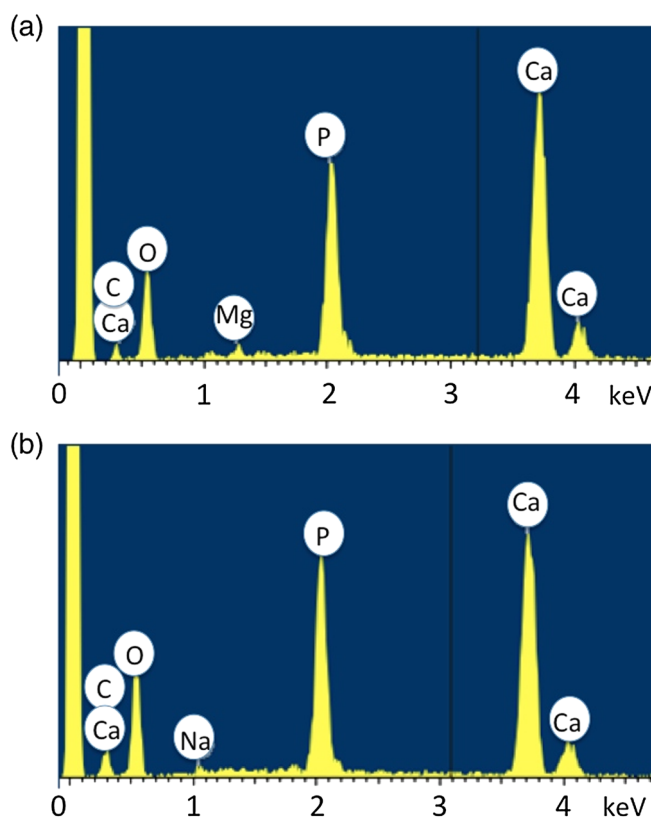
In all phantoms,  $f_{\text{P}}$  was overestimated more than  $f_{\text{Ca}}$  using EDX (Figure 5). In addition to the low effect of ZAF correction, a possible reason for this could be the interference between the P  $\text{K}_{\alpha}$  line (2.10 keV), and the silicon K escape peaks (of the Si(Li) detector) because of the Ca  $\text{K}_{\alpha}$  and  $\text{K}_{\beta}$  lines (1.95 and 2.27 keV). However, this source of error is only small because the peak areas of Ca and P are comparable<sup>[8]</sup>. Furthermore, fluorescence can significantly alter the relative amounts of characteristic radiation coming from alloys or compounds, particularly when elements with quite similar atomic numbers are present<sup>[21]</sup>. However, it is not expected that fluorescence significantly affected our results, because of its low effect in this energy region.

The errors in  $f_{\text{Ca}}$  and  $f_{\text{P}}$  were propagated into the calculation of the Ca/P ratio. Because of an overestimation of  $f_{\text{P}}$  in comparison with  $f_{\text{Ca}}$ , an underestimation is always made on the calculation of the Ca/P ratio, resulting in a mean/maximum accuracy of  $-0.07/-0.11$  in the Ca/P ratio.

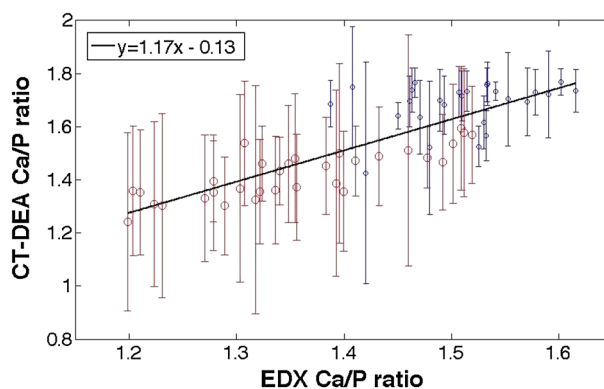
### Samples

Figure 6 shows examples of the spectra acquired from (a) a healthy bone sample and (b) an IMO bone sample. EDX shows the presence of the chemical components in the sample; calcium, phosphorus, carbon, oxygen, magnesium, and sodium are all expected to be present in bone apatite<sup>[22]</sup>. The relative difference in heights of the Ca and P peaks in (a) is greater than in (b), reflecting a higher Ca/P ratio.

The Ca/P ratio results in healthy bone samples using EDX were within the range of 1.39–1.62 (x-axis of plot in Figure 7). The Ca/P molar ratio for the stoichiometric hydroxyapatite is 1.67<sup>[4]</sup>. This underestimation of Ca/P ratio by the SEM system is not surpris-



**Figure 6.** Examples of the spectra acquired from (a) a healthy bone sample and (b) an inflammation-mediated osteoporotic bone sample.



**Figure 7.** CT dual energy analysis Ca/P ratio versus energy-dispersive X-ray Ca/P ratio of 58 regions of interest in eight samples; four healthy (blue) and four osteoporotic (red). Error bars represent the standard deviation in one voxel.

ing because, as shown by the bone phantom results of EDX,  $f_{\text{P}}$  is systematically overestimated compared with  $f_{\text{Ca}}$ .

The Ca/P ratio results in IMO bone samples using EDX were within the range of 1.19–1.52 (x-axis of plot in Figure 7). Comparing the difference of the Ca/P ratios of the healthy and IMO areas, using a Student's *t*-test, a *p*-value of  $< 0.05$  (Table 2) was given. From this, it can be concluded that there is a statistically significant difference in the Ca/P ratios of the healthy and IMO bone sample areas. These results are in agreement with other studies, where a statistically significant difference was found in the Ca/P ratio between healthy and IMO bones<sup>[4,5,11]</sup>.

**Table 2.** The Ca/P ratio *t*-test results of the collagen-free bone samples using scanning electron microscopy and CT dual energy analysis.

Variable	SEM		CT-DEA	
	Healthy	IMO	Healthy	IMO
Mean	1.51	1.36	1.68	1.42
Observations	26	32	26	32
<i>p</i> -value	<0.0001		<0.0001	

IMO, inflammation-mediated osteoporotic.

### CT-DEA performance for Ca/P ratio assessment in bone apatite

The Ca/P ratio results using CT-DEA were within the range of 1.43–1.77 and 1.24–1.59 (*y*-axis of plot in Figure 7) for healthy and IMO bone samples, respectively. Comparing with the EDX results; 1.39–1.62 for healthy samples and 1.20–1.52 for IMO samples, it can be concluded that an overestimation is made by CT-DEA. This systematic error is because of non-perfect fit of the pre-defined relations of  $F(Z_{eff})$  (ratio of low and high energy CT values for one voxel) to  $Z_{eff}$  (effective atomic number) and  $Z_{eff}$  to  $m_L$  (low energy mass attenuation coefficient) of the phantoms that were used to calibrate the technique<sup>[6]</sup>. At present, approximations of the aforementioned mathematical relations are required in CT-DEA for bone material decomposition. This is due to the fact that the exact chemical composition of biological apatite is diverse and not known with sufficient accuracy to enable the construction of a precise look-up table of  $F(Z_{eff})$  to  $Z_{eff}$  and  $Z_{eff}$  to  $m_L$ .

CT dual energy analysis provided Ca/P ratio values within a mean absolute/percentage difference from the EDX results of  $0.11 \pm 0.08 / 8 \pm 6\%$ . Linear regression analysis in the plot of CT-DEA Ca/P ratio results versus EDX Ca/P ratio results of the same areas provided the value for the coefficient of determination;  $R^2 = 0.69$ .

The noise in CT-DEA low and high energy images introduces an error in the Ca/P ratio results. It is important to note that this error only partly expresses the magnitude of the error bars in Figure 7, otherwise, the reader might be misled on the precision of the CT-DEA results. The magnitude of the error bars is also expressed by the non-homogeneous spatial distribution of the Ca/P ratio in the ROIs. For example, in one ROI, of approximately 0.15–0.23 mm<sup>2</sup> area, the Ca/P ratio varies from place to place, therefore the mean Ca/P ratio includes some deviation from the minimum and maximum Ca/P ratio in the same region. This is supported by the fact that the magnitude of the error bars, and thus the variation in the Ca/P ratio is higher in IMO bone sample ROIs (red lines in Figure 7) than in healthy bone sample ROIs (blue lines in Figure 7). This suggests a higher non-homogeneity of Ca/P ratio in IMO areas, which, as has been shown in previous studies<sup>[4]</sup>, could be a criterion for osteoporosis.

The results of the accuracy of CT-DEA of Ca/P ratio measurements in bone apatite were very dependent on the successful mapping of the images from the two imaging systems. One of the causes of the lack of 0.31 in the coefficient of determination of the plot in Figure 7, is the non-perfect mapping of the images, because of the lack of comparable alignment of the sample with the pixels of the two systems. It was technically difficult to evaluate the error introduced by the non-perfect mapping, because it is partly dependent on the spatial distribution of the Ca/P ratio in the ROIs.

In addition, even though the surface area of each region was almost the same between the two systems, the depth within the sample to which the EDX Ca/P ratio results correspond to was estimated to be 4  $\mu\text{m}$ , compared with the CT-DEA, which was preset as 96  $\mu\text{m}$ . Further study is required to investigate how a higher spatial resolution by the CT-DEA system (maximum resolution in the depth direction possible is 16  $\mu\text{m}$ , which is the thickness of a microCT slice), which would decrease the signal to noise ratio, would affect the correlation of the Ca/P ratio results between the two imaging systems.

Table 2 shows the results of a Student's *t*-test on the assessment of the statistical significance in the difference in healthy and IMO bone samples using the two imaging techniques. As in the case of EDX, a statistically significant difference ( $p < 0.05$ ) was found between healthy and IMO bone samples using CT-DEA.

Because of the undetermined uncertainties introduced in the analysis by image mapping and depth interaction of electrons, it cannot be concluded to what absolute accuracy the Ca/P ratio can be measured in real bone apatite using CT-DEA. However, a value of  $R^2 = 0.69$  in the fit of CT-DEA Ca/P ratio versus EDX Ca/P ratio and a mean difference in the Ca/P ratio between the two techniques of  $0.11 \pm 0.08$  suggests sufficient confidence in the experimental capabilities of technique.

## Conclusions

The results of this study show that CT-DEA can provide the expected trend in the assessment of the spatial distribution of the Ca/P ratio in bone apatite. The uncertainties in the absolute values of the Ca/P ratio by CT-DEA cannot be currently quantified. However, they can be improved if a more wide and accurate database of the chemical composition of bone is used.

Even though there are still possible improvements that can be made in the CT-DEA technique, it has been so far shown that it can provide valuable 3D information on the comparison between healthy and osteoporotic bone. Furthermore, it has the big advantage over EDX for its non-invasive Ca/P ratio assessment in bone. This could potentially help in studying the 3D spatial distribution of Ca/P ratio and its correlation to bone quality in human healthy and osteoporotic bone.

## Acknowledgements

A. Hadjipanteli would like to acknowledge Engineering and Physical Sciences Research Council (EPSRC, UK) for the PhD studentship funding for this project. The authors thank Dr J. McClelland for his help in the use of NifTK platform, Mr G. Cole for his help in the use of EDX and Dr I. Balatsoukas and Mrs A. Lani, MD, for animal handling and bones dissection.

## References

- [1] J. A. Kanis, C. Glu, An update on the diagnosis and assessment of osteoporosis with densitometry, *Osteoporosis Int.* **2000**, *11*, 192–202.
- [2] H. Bolotin, H. Sievanen, Inaccuracies inherent in dual-energy X-ray absorptiometry in vivo bone mineral density can seriously mislead diagnostic/prognostic interpretations of patient-specific bone fragility, *J. Bone Miner. Res.* **2011**, *16*, 799–805.
- [3] G. J. Kazakia, S. Majumdar, New imaging technologies in the diagnosis of osteoporosis, *Rev. Endocr. Metab. Dis.* **2006**, *7*, 67–74.

- [4] M. Tzaphlidou, R. Speller, G. Royle, J. Griffiths, A. Olivo, S. Pani, R. Longo, High resolution Ca:P maps of bone architecture in 3D synchrotron radiation microtomographic images, *Appl. Radiat. Isot.* **2005**, *62*, 569–575.
- [5] G. Fountos, M. Tzaphlidou, E. Kounadi, D. Glaros, In vivo measurement of radius calcium/phosphorus ratio by X-ray absorptiometry, *Appl. Radiat. Isot.* **1999**, *51*, 273–278.
- [6] A. Hadjipanteli, N. Kourkoumelis, P. Fromme, A. Olivo, J. Huang, R. Speller, A new technique for the assessment of the 3D spatial distribution of the calcium/phosphorus ratio in bone apatite, *Physiol. Meas.* **2013**, *34*, 1399–1410.
- [7] K. Akesson, M. D. Grynopas, R. G. V. Hancock, R. Odselius, K. J. Obrant, Energy-dispersive X-ray microanalysis of the bone mineral content in human trabecular bone: a comparison with ICPEs and neutron activation analysis, *Calcif. Tissue Int.* **1994**, *55*, 236–239.
- [8] M. J. Bailey, S. Coe, D. M. Grant, G. W. Grime, C. Jaynes, Accurate determination of the Ca:P ratio in rough hydroxyapatite samples by SEM-EDS, PIXE and RBS - a comparative study, *X-Ray Spectrom.* **2009**, *38*, 343–347.
- [9] H. Benhayoune, D. Charlier, E. Jallot, P. Laquerriere, G. Balossier, P. Bonhomme, Evaluation of the Ca:P concentration ratio in hydroxyapatite by STEM-EDXS: influence of the electron irradiation dose and temperature processing, *J. Phys. D: Appl. Phys.* **2001**, *34*, 141–147.
- [10] J. P. Cassella, N. Garrington, T. C. B. Stamp, S. Y. Ali, An electron-probe X-ray microanalytical study of bone mineral in osteogenesis imperfecta, *Calcif. Tissue Int.* **1995**, *56*, 118–122.
- [11] N. Kourkoumelis, I. Balatsoukas, M. Tzaphlidou, Ca:P concentration ratio at different sites of normal and osteoporotic rabbit bones evaluated by Auger and energy dispersive X-ray spectroscopy, *J. Biol. Phys.* **2011**, *38*, 279–291.
- [12] N. Kourkoumelis, A. Lani, M. Tzaphlidou, Infrared spectroscopic assessment of the inflammation-mediated osteoporosis (IMO) model applied to rabbit bone, *J. Biol. Phys.* **2012**, *38*, 632–635.
- [13] C. M. Payne, D. W. Crome, Limitations of ZAF correction factors in the determination of calcium/phosphorus ratios: important forensic science considerations relevant to the analysis of bone fragments using scanning electron microscopy and energy-dispersive x-ray microanalysis, *J. Forensic Sci.* **1990**, *35*, 560–568.
- [14] P. Roschger, P. Fratzl, K. Klaushofer, G. Rodan, Mineralization of cancellous bone after alendronate and sodium fluoride treatment: a quantitative backscattered electron imaging study on minipig ribs, *Bone* **1997**, *20*, 393–397.
- [15] P. Sarathchandra, M. V. Kayser, S. Y. Ali, Abnormal mineral composition of osteogenesis imperfecta bone as determined by electron probe X-ray microanalysis on conventional and cryosections, *Calcif. Tissue Intern.* **1999**, *65*, 11–15.
- [16] E. Bolton, Y. Wang, P. A. Thiessen, S. H. Bryant, PubChem: Integrated platform of small molecules and biological activities, in *Annu. Rep. Comput. Chem.*, American Chemical Society, Washington, DC, **2008**, pp. 4, chapter 12.
- [17] K. J. Armour, K. E. Armour, Bone research protocols: inflammation-induced osteoporosis, The IMO model, in *Methods in Molecular Medicine*, Totowa, NJ: Humana Press Inc., New York, **2003**, pp. 80.
- [18] E. G. Vajda, J. G. Skedros, R. D. Bloebaum, Errors in quantitative backscattered electron analysis of bone standardized by energy-dispersive X-ray spectrometry, *Scanning* **1998**, *20*, 527–535.
- [19] F. Miculescu, L. Ciocan, Effect of heating process on micro structure level of cortical bone prepared for compositional analysis, *Dig. J. Nanomat. Bios.* **2011**, *6*, 225–233.
- [20] M. Raspanti, S. Guizzardi, V. De Pasquale, D. Martini, A. Ruggeri, A, Ultrastructure of heat-deproteinated compact bone, *Biomaterials* **1994**, *15*, 433–437.
- [21] P. J. Goodhew, J. Humphreys, R. Beanland, *Electron Microscopy and Snalysis*, Taylor and Francis Inc., CRC Press, London, **2011**.
- [22] S. V. Dorozhkin, Calcium orthophosphate-based biocomposites and hybrid biomaterials, *Journal of Mater. Sci.* **2009**, *44*, 2343–2387.